THE JOURNAL OF PHYSICAL CHEMISTRY LETTERS
A JOURNAL OF THE AMERICAN CHEMICAL SOCIETY

pubs.acs.org/JPCL Letter

Probing Torsional Tunneling in Al_2H_4 via Anion Photoelectron Spectroscopy

Rui Zhang, Qihan Liu, Jiayi Chen, Wenru Jie, and Chuangang Ning*

Cite This: J. Phys. Chem. Lett. 2026, 17, 6405−6410 Read Online

ACCESS | Metrics & More | Article Recommendations | Supporting Information

ABSTRACT: This study investigates the tunneling dynamics associated with the torsional transition in the Al_2H_4 molecule by photodetaching its anionic counterpart, $Al_2H_4^-$. The stable structure of $Al_2H_4^-$ exhibits D_{2h} symmetry, whereas neutral Al_2H_4 adopts a D_{2d} symmetric configuration. According to the Franck−Condon principle, the tunneling dynamics across the torsional barrier in Al_2H_4 can be directly probed through the high-resolution photoelectron spectroscopy of $Al_2H_4^-$ anions. Our Franck−Condon factor simulations, based on solutions to the Mathieu equation that incorporate tunneling effects, successfully reproduce the experimental observations. The approach presented here is also applicable to other molecular systems involving intramolecular torsion.

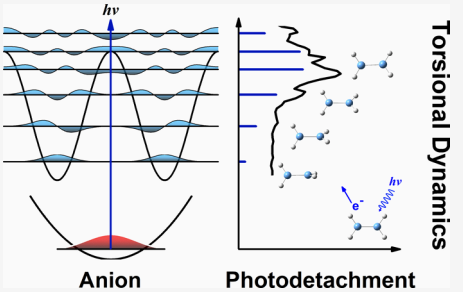

The tunneling effect[1,2] is a fundamental physical phenomenon that distinguishes the quantum world from the classical one. It frequently occurs during the instantaneous isomerization involving a reaction barrier.[3] As a special form of isomerization, molecular internal torsion exhibits periodic conformational interconversion, passing through transition states along the torsional coordinate.[4,5] Ethane serves as a textbook example: its CH_3 groups rotate around the central C−C bond, causing the molecule to alternate between the unstable eclipsed conformation and the preferred staggered conformation.[6−8] Many organic and biological molecules exhibit significant and diverse quantum tunneling effects during the hindered internal rotation of methyl (−CH_3) or hydroxyl (−OH) groups. The dynamics of such tunneling processes have been extensively studied in gas-phase species such as the carboxyl radical (HOCO),[9] *cis*-HCOOH,[10] phenol (C_6H_5OH),[11] methylhydroxycarbene ($H_3C−C−OH$),[12] and propofol,[13] primarily using infrared (IR) and microwave spectroscopic techniques.

However, conventional infrared and microwave spectroscopy mainly probes stable neutral species, accessing internal rotation states with energies near the bottom of the periodic potential well, rather than across the entire potential barrier. Furthermore, not all internal rotations are IR- or microwave-active due to electric-dipole selection rules.

When a stable anion adopts a geometry resembling the transition state on the neutral molecule's torsional barrier, detailed information about the torsional dynamics is encoded in its vibrationally resolved photoelectron spectrum. This anion photodetachment strategy for probing transition states, pioneered by Neumark, Lineberger, and their co-workers in classic studies of vinylidene,[14,15] cyclooctatetraene,[16] and the F + H_2 reaction,[17] is now extended to the torsional isomerization system. During photodetachment, the anion emits its excess electron, and its vibrational wave function is projected vertically onto the neutral molecule's wave functions—particularly those localized within the barrier region—thereby directly sampling quantum tunneling dynamics. Crucially, this anion photodetachment approach enables direct characterization of the torsional transition state, a target that is otherwise inaccessible to IR spectroscopy due to the fleeting nature of transition states.[18]

Recently, cryogenic slow electron velocity-map imaging (cryo-SEVI), a high-resolution variant of anion photodetachment spectroscopy, has emerged as a powerful tool for experimentally characterizing neutral short-lived species and transient processes. By achieving an energy resolution as high as a few cm^{-1} near the photodetachment threshold, this method is ideally suited for resolving complex vibrational structures. SEVI has been successfully used to characterize chemical reaction dynamics including F+H_2,[19] F + CH_3OH,[20] F+NH_3[21,22] and H+NH_3.[23]

In this work, we employ SEVI to investigate the torsional isomerization dynamics of Al_2H_4. Aluminum-containing clusters have long been of interest due to their distinctive aluminum−aluminum bonds[24−27] and potential applications in hydrogen storage[28] and catalysis.[29] Previous theoretical calculations have identified multiple stable conformers for both neutral and anionic Al_2H_4.[30] Among these, the neutral Al_2H_4 (D_{2d}) is particularly intriguing: it features a covalent yet

Received: April 7, 2026
Revised: May 13, 2026
Accepted: May 22, 2026
Published: May 28, 2026

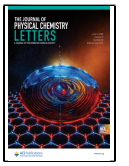

https://doi.org/10.1021/acs.jpclett.6c01123
J. Phys. Chem. Lett. 2026, 17, 6405−6410

flexible Al−Al bond and exhibits internal rotation of the two AlH_2 groups.[31,32] The photodetachment of $Al_2H_4^-$ (D_{2h}) anion leads to the neutral Al_2H_4 at a transition state connecting the stable Al_2H_4 (D_{2d}) through the AlH_2-group rotation around the Al−Al bond. Moreover, a quantum tunneling across this transition state is highly preferred due to the low barrier height of 355 cm^{-1}. Crucially, the stable $Al_2H_4^-$ (D_{2h}) anion exhibits a geometry similar to that of the neutral transition state, allowing direct experimental observation of the tunneling dynamics via photodetachment of $Al_2H_4^-$ anion. The simple and symmetric structure reduces computational cost and facilitates Franck−Condon factor (FCF) simulations of wave function overlap between the anionic ground state and the tunneling-accessible states within the torsional barrier. As a result, $Al_2H_4^-$ anion represents an ideal model system for exploring quantum tunneling dynamics in intramolecular torsion.

OBSERVATION OF TORSIONAL TRANSITION STATE

Neutral Al_2H_4 exhibits three stable conformers: **1** (C_{3v}), **2** (C_{2v}) and **3** (D_{2d}). Among these, conformer **3** (D_{2d}) undergoes hindered internal rotation around the Al−Al bond, periodically interconverting between itself and the torsional transition state **4** (D_{2h}) every 90°. This transition state is calculated to lie about 355 cm^{-1} above **3** (D_{2d}). Anionic $Al_2H_4^-$ has two stable structures: $\mathbf{2}^-$ (C_{2v}) and $\mathbf{4}^-$ (D_{2h}). Photodetachment of these two anionic species directly reveals the structures of neutral **2** (C_{2v}) and **4** (D_{2h}). The structures of neutral and anionic Al_2H_4, along with their calculated relative energies, are shown in Figure 1. Molecular orbital analysis of **3**, **4** and $\mathbf{4}^-$ reveals why

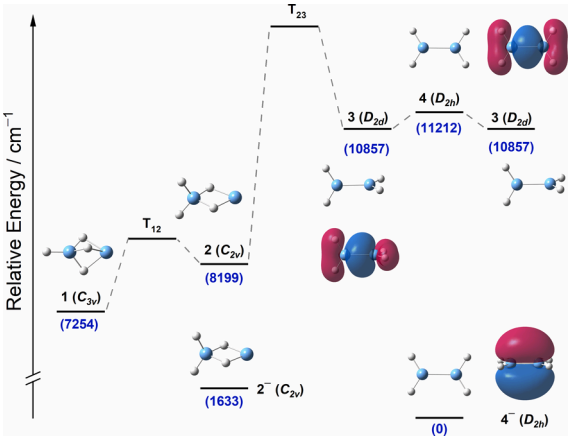

Figure 1. Relative calculated energies with zero-point energy corrections of the neutral and anionic Al_2H_4 conformers. Energies are referenced to the most stable anionic conformer $\mathbf{4}^-$ (D_{2h}). The neutral conformer **4** (D_{2h}) is the transition state of the intramolecular AlH_2 torsion process of **3** (D_{2d}). $\mathbf{T_{12}}$ and $\mathbf{T_{23}}$ are the other transition states between neutral Al_2H_4 conformers. Optimized structures are illustrated for the anionic and neutral Al_2H_4 in light blue (Al) and white (H). The highest occupied molecular orbitals (HOMO) of conformers **3**, **4** and $\mathbf{4}^-$ are also depicted around their structures.

the photodetachment of $\mathbf{4}^-$ anion can trigger the interconversion between **4** (D_{2h}) and **3** (D_{2d}). In conformer **3**, the distance between two electron clouds localized at $-AlH_2$ groups is longer than in conformer **4**. Consequently, the torsional repulsion is smaller, rendering **3** more stable than **4**. Generally, the staggered-type torsional conformers are more stable than the eclipsed-type.[7,8] However, the excess electron in $\mathbf{4}^-$ occupies a delocalized π orbital, which makes the planar structure more stable (Figure 1), and creates a deep potential well at D_{2h} symmetry that suppresses torsion. This orbital-driven stabilization enables direct experimental access to the transient transition state **4** through photodetachment spectroscopy of $\mathbf{4}^-$.

Figure 2 shows the cryo-SEVI overview spectrum of $Al_2H_4^-$ anions acquired at a wavelength of 600 nm. The spectrum

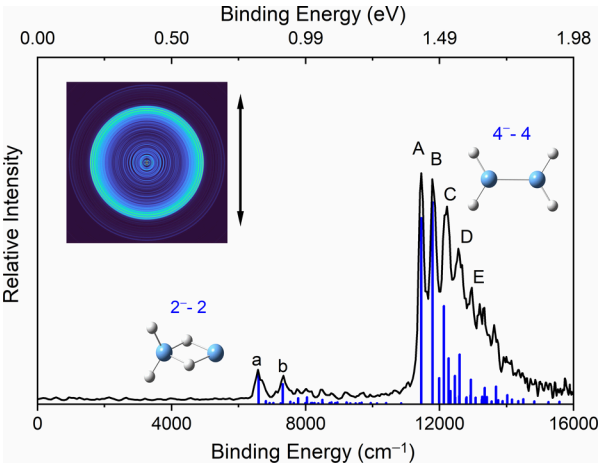

Figure 2. Photoelectron image and full spectrum of $Al_2H_4^-$. The double-headed arrow indicates the polarization of the detachment laser. Two bands are assigned to photodetachment transitions $\mathbf{2}^-$−**2** and $\mathbf{4}^-$−**4**, respectively. The blue vertical lines indicate Franck−Condon simulations. The geometric structures of two $Al_2H_4^-$ isomers, $\mathbf{2}^-$ and $\mathbf{4}^-$, are also plotted.

reveals photodetachment transitions originating from two distinct stable anionic conformers of $Al_2H_4^-$, $\mathbf{2}^-$ (C_{2v}) and $\mathbf{4}^-$ (D_{2h}). The higher-energy C_{2v} anionic isomer cannot transform into the D_{2h} anionic isomer under the current experimental conditions due to a high interconversion barrier. To assign the peaks, we conducted FCF simulations. As indicated by the vertical spikes, the simulations exhibit excellent agreement with the experimental spectra, which are notably different from previous theoretical predictions.[30] Peaks ***a*** and ***A*** correspond to transitions from the ground states of $Al_2H_4^-$ anion in C_{2v} and D_{2h} symmetries to their respective neutral ground states. The measured binding energies of peaks ***a*** and ***A***, which correspond to the vertical electron affinities of Al_2H_4 in each symmetry, were determined to be 6590(138) cm^{-1} (C_{2v}) and 11454(208) cm^{-1} (D_{2h}), respectively. These experimental values are consistent with our theoretical calculations, 6566 and 11212 cm^{-1} for the respective symmetries. The fundamental frequency of the AlH_2 stretching modes in transition state **4** (D_{2h}) was experimentally determined to be 347 cm^{-1} by comparing the positions of peaks ***A*** and ***B***, in excellent agreement with the theoretical results of 348 cm^{-1}. A higher-resolution photoelectron spectrum of the $\mathbf{2}^-$ (C_{2v}) anion, acquired near its photodetachment threshold, is provided in the Supporting Information. All observed peaks and their assignments are also summarized in Table S5. It should be noted that the FCF simulation for the D_{2h} symmetry in Figure 2 temporarily excluded the AlH_2 torsional mode because the corresponding neutral transition state **4** (D_{2h}) has an imaginary frequency associated with this mode. A detailed analysis of the AlH_2 torsional mode will be presented in the subsequent subsection.

https://doi.org/10.1021/acs.jpclett.6c01123
J. Phys. Chem. Lett. 2026, 17, 6405−6410

Calculation of Torsional Energy Levels

The torsional motion of Al_2H_4 is significantly slower than its other vibrational motions, permitting the torsional energy levels to be calculated approximately by solving the Schrödinger equation with all other vibrational coordinates fixed at their equilibrium values. The torsional interconversion between D_{2d} and D_{2h} conformers is periodic with a period of π. Accordingly, the torsional potential energy V, as a function of torsional angle τ, can be expressed as

$$V(\tau) = \frac{V_2}{2}(1 + \cos 2\tau)$$

where V_2 represents the relative energy difference between these two configurations of Al_2H_4. High-level UCCSD(T)-F12 calculations performed with the MOLPRO computational package[33] yield a value of V_2 = 410.33 cm^{-1}. This value includes a correction for the zero-point energy of all modes except torsion. Substituting this torsional potential $V(\tau)$ into the one-dimensional Schrödinger equation yields the angular Mathieu equation

$$\psi'' + (\lambda - 2q \cos 2\tau)\psi = 0$$

Here, ψ is the wave function of the torsional mode. The dimensionless parameters λ and q are defined as $\lambda = \frac{E}{F} - \frac{V_2}{2F}$ and $q = \frac{V_2}{4F}$, where $F \approx \frac{\hbar^2}{2I_r}$ is the kinetic factor under the rigid-top approximation,[34,35] I_r is the reduced moment of inertia for the two AlH_2 groups, and E is the torsional energy. Therefore, determining the torsional energy levels E_n and the wave function ψ_n is equivalent to solving the characteristic Mathieu equation for its eigenvalues and eigenfunctions.

Each calculated torsional energy level splits into two sublevels due to the quantum tunneling effect, which mixes states otherwise localized in one potential well. These symmetric and antisymmetric sublevels are all plotted in Figure 3. Their corresponding wave functions are depicted in purple and blue, respectively. The symmetric wave function possesses a lower energy than its antisymmetric counterpart.

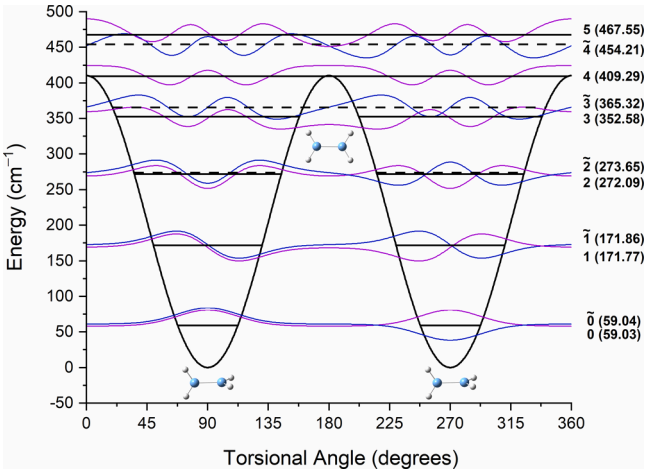

Figure 3. Torsional potential energy curve and energy levels for the AlH_2 internal torsion in neutral Al_2H_4. The energy is referenced to the potential minimum. Each torsional level splits into doublets due to quantum tunneling. Solid and dashed black lines indicate energy sublevels with a symmetric (purple) and an antisymmetric (blue) eigenfunction, respectively.

Since the $Al_2H_4^-$ anions were cooled down and thermalized to their vibrational ground state via buffer gas cooling in the cryogenic ion trap, only the wave function of the anionic ground state is plotted in Figure 4(a). The neutral torsional

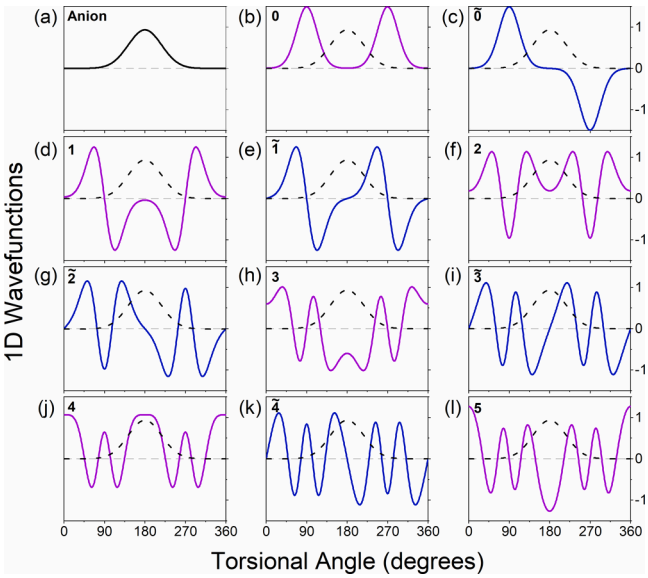

Figure 4. (a) Ground-state torsional wave function of the anion. (b)−(l) Symmetric (purple) and antisymmetric (blue) torsional wave functions of neutral Al_2H_4, labeled according to their quantum states from Figure 3. The dashed line in each panel is the wave function of anion for showing the overlap with neutral wave functions.

wave functions are plotted against the anionic wave function in Figure 4(b)−(i) to show their overlap. The calculated energy splitting between the symmetric and antisymmetric ground states is approximately 0.0021 cm^{-1}, corresponding to a tunneling rate of 63 MHz for the Al_2H_4 molecule through the torsional barrier. The tunneling rate increases with higher torsional energy levels. As the energy levels surpass the barrier height, AlH_2 groups become a nearly free rotator. The calculated values for all torsional energy levels are summarized in Table 1.

Table 1. Calculated Torsional Energy Levels of Neutral Al_2H_4 (cm^{-1})

Symmetric Level	Energy[a]	Antisymmetric Level	Energy
0	59.03	0̃	59.04
1	171.77	1̃	171.86
2	272.09	2̃	273.65
3	352.58	3̃	365.32
4	409.29	4̃	454.21
5	467.55	5̃	552.35

[a]The energy is referenced to the potential minimum **3** (D_{2d}).

Observation and Simulation of Torsional Dynamics

To resolve the energy levels related to the torsional mode of Al_2H_4, the detachment laser energy was tuned near the threshold of peak A. As shown in Figure 5, peak A exhibits several finer features, labeled A_0−A_5 with an energy gap ∼70 cm^{-1}. To assign the finer features, we employed FCF simulations. It should be noted that the conventional FCF programs based on the harmonic oscillator model are not applicable here. Instead, we directly calculate the overlap f_c

https://doi.org/10.1021/acs.jpclett.6c01123
J. Phys. Chem. Lett. 2026, 17, 6405−6410

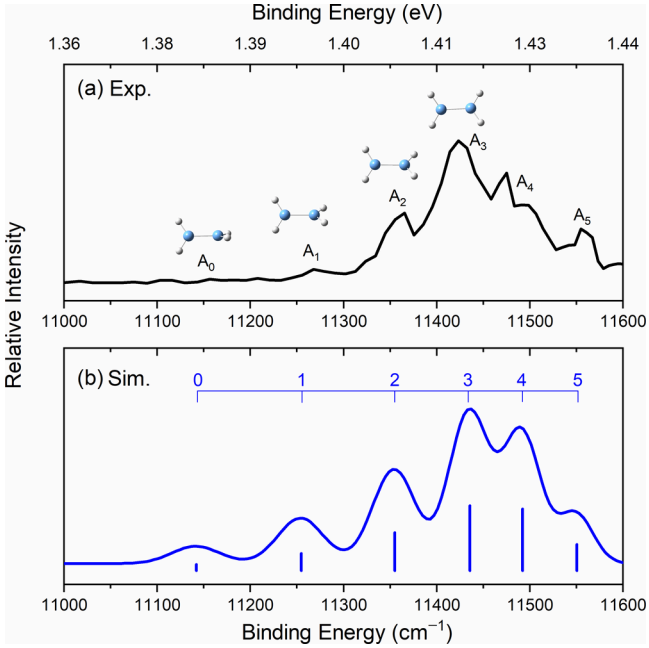

Figure 5. (a) High-resolution photoelectron spectrum reveals the AlH_2 internal torsion states of neutral Al_2H_4. (b) Simulated photodetachment electron spectrum, based on the calculated Franck–Condon factors using the Mathieu equation. The labels at the top indicate the assignment of the torsional state.

between the anionic ground wave function and the neutral torsion wave function generated using the Mathieu equation, as shown in Figure 4. The observed intensity of each fine feature is proportional to $|f_c|^2$. The dominant FC overlap contribution is from the neutral wave functions within the tunneling region since the anionic ground-state wave function has its greatest amplitude near the top of the neutral torsional barrier. Since the anionic ground state is of even symmetry, only transitions to symmetric (even) neutral vibrational states have significant intensity, while transitions to antisymmetric (odd) states are formally forbidden and yield near-zero intensity. Therefore, all observed peaks are assigned as transitions to the neutral symmetric torsional sublevels.

As shown in Figure 5, the FCF simulation reproduces the experimental spectrum well. The FCF simulation reveals that peaks A_0–A_3 correspond to torsional levels below the barrier, which are classically forbidden. The relative intensity of A_0–A_3 represents the probability of the torsional interconversion due to quantum tunneling. In contrast, peaks A_4 and A_5 represent torsional eigenstates above the barrier, where Al_2H_4 behaves like a free internal rotator, rapidly switching between two conformers. The relatively well-resolved peak A_2 served as the reference, yielding a measured binding energy of 11360(45) cm^{-1}. By subtracting the calculated torsional level difference of 213 cm^{-1} between the torsional second excited and ground states, we indirectly obtain a refined adiabatic electron affinity of 11147(46) cm^{-1} for Al_2H_4. The energy splitting between torsional sublevels cannot be resolved in the current experiment, and the existence of tunneling splitting was inferred from the Mathieu-equation-based simulation. The measured binding energies for these torsional transitions, alongside their calculated values, are summarized in Table 2.

The photodetachment of $Al_2H_4^-$, combined with the FC simulation based on solutions to the Mathieu equation, effectively captures the transient torsional dynamics of Al_2H_4.

Table 2. Binding Energies of Photodetachment Transitions for Torsional Mode

Peaks	Exptl eBE (cm^{-1})	Exptl Shift (cm^{-1})[a]	Theor Shift (cm^{-1})	Assignment[b]
A_0			−213	0
A_1	11266(62)	−94	−100	1
A_2	11360(45)	0	0	2
A_3	11427(59)	67	80	3
A_4	11499(53)	139	137	4
A_5	11559(26)	199	195	5

[a]Since peak A_0 is too weak to determine its position in the current experiment, the energy shift is referenced to the binding energy of peak A_2. [b]All transitions are from the anionic ground state to the different neutral torsional symmetric states.

Internal torsion is ubiquitous in nature, ranging from the isomerization of single molecular groups to the double helix of DNA and the folding of protein polypeptide chains. Observing such torsion via negative ion photodetachment represents a powerful approach to significantly advance our understanding of torsional dynamics. $Al_2H_4^-$ is a stable anion with a simple structure. It may also serve as a good model system to answer the question: Does the tunneling process take time?[36−39] In a pump–probe experiment, a short laser pulse could detach $Al_2H_4^-$ and create a transition state under the barrier; then, a second short laser pulse could probe the geometrical evolution of the nascent neutral Al_2H_4 using an experimental technique such as Coulomb Explosion,[40] or Mega-electronvolt Ultrafast Electron Diffraction (MeV-UED).[41]

In conclusion, we have observed the transient torsional transition state by photodetachment of $Al_2H_4^-$ anions. The FCF simulations based on the torsional wave function overlaps successfully reproduced the experimental results, revealing that the torsional internal conversion occurs in both the tunneling region and the free rotator region. Compared with the conventional IR spectroscopy, which typically probes only the energy levels near the torsional potential well bottom, the anion photodetachment method can probe both the tunneling region below the barrier and the free rotator region above the barrier. The present work demonstrates the successful application of anion photodetachment for studying the dynamics of the fleeting torsional transition states.

METHODS

Experimental Methods

The experiments were performed using our slow-electron velocity-map imaging apparatus equipped with a cryogenically controlled ion trap (cryo-SEVI).[42−44] Aluminum–hydrogen cluster ions were generated by laser ablation of a rotating and translating aluminum target in the presence of hydrogen gas. The hydrogen gas was pulsed and directed toward the aluminum target before each ablation laser shot via a pulse valve, with the timing sequence optimized to maximize the anion beam intensity. The produced anions were guided by a radio frequency (RF) hexapole and stored in an RF octupole cryogenic ion trap held at 15 K.[45] After cooling for 45 ms via collisions with the buffer gas (20% H_2 and 80% He) in the ion trap, the anions were thermalized to their vibrational and electronic ground state, with only the lowest few rotational excited states populated. Subsequently, they were pulsed out of the ion trap and analyzed by a time-of-flight (TOF) mass spectrometer.[46] The mass-selected $Al_2H_4^-$ anions were then photodetached at various photon energies using a tunable optical-parametric-oscillator (OPO) laser in the photodetachment region. The outgoing photoelectrons were analyzed via a velocity-map imaging (VMI) spectrometer.[47,48] Their velocity

https://doi.org/10.1021/acs.jpclett.6c01123
J. Phys. Chem. Lett. 2026, 17, 6405−6410

distributions were reconstructed from the raw projected images using the Maximum Entropy Velocity Legendre Reconstruction (MEVELER) method.[49,50]

Computational Methods

The geometrical optimization and energy calculations of all neutral and anionic Al_2H_4 conformers were performed with the MOLPRO computational package[33] at CCSD(T)-F12/aug-cc-pVTZ level. The relative energies of all neutral and anionic Al_2H_4 conformers are listed in Supplementary Table 3. The Franck−Condon factor simulations for modes other than the torsion were conducted using the ezFCF program.[51] For the torsional mode, the simulation incorporated anharmonic effects. Specifically, the periodic torsional potential

$$V(\tau) = \frac{V_2}{2}(1 + \cos 2\tau)$$

was used instead of a harmonic potential. The harmonic approximation would confine the vibrational wave function to a single potential well, yielding no tunneling. In contrast, solving the Mathieu equation for this periodic potential allows the wave function to delocalize across the torsional barrier, producing symmetric and antisymmetric eigenstates whose splitting corresponds to quantum tunneling. The initial state was described by the harmonic oscillator ground-state wave function of the anion. The final neutral torsional wave functions, which are critical for describing the tunneling dynamics, were obtained by solving the Mathieu equation for its eigenfunctions, providing a more accurate treatment of the large-amplitude motion than the harmonic approximation. The photodetachment simulation of peak intensities also takes into account the Wigner threshold law,[52] and the simulated peak widths were convoluted with a Gaussian function accounting for instrumental resolution and rotational broadening.

■ ASSOCIATED CONTENT

Data Availability Statement

The data that support the findings of this study are available from the corresponding author upon reasonable request.

Supporting Information

The Supporting Information is available free of charge at https://pubs.acs.org/doi/10.1021/acs.jpclett.6c01123.

High-resolution photoelectron spectrum of 2^- (C_{2v}), optimized Cartesian coordinates of neutral and anionic Al_2H_4 conformers, relative energies of neutral and anionic Al_2H_4 conformers, harmonic frequencies of neutral and anionic Al_2H_4 conformers, and electron binding energies, widths, shifts and assignments of all peaks (PDF)

■ AUTHOR INFORMATION

Corresponding Author

Chuangang Ning − *Department of Physics, State Key Laboratory of Low Dimensional Quantum Physics, Frontier Science Center for Quantum Information, Tsinghua University, Beijing 100084, China;* orcid.org/0000-0002-3158-1253; Email: ningcg@tsinghua.edu.cn

Authors

Rui Zhang − *Department of Physics, State Key Laboratory of Low Dimensional Quantum Physics, Frontier Science Center for Quantum Information, Tsinghua University, Beijing 100084, China;* orcid.org/0000-0001-9080-4528

Qihan Liu − *Department of Physics, State Key Laboratory of Low Dimensional Quantum Physics, Frontier Science Center for Quantum Information, Tsinghua University, Beijing 100084, China*

Jiayi Chen − *Department of Physics, State Key Laboratory of Low Dimensional Quantum Physics, Frontier Science Center for Quantum Information, Tsinghua University, Beijing 100084, China*

Wenru Jie − *Department of Physics, State Key Laboratory of Low Dimensional Quantum Physics, Frontier Science Center for Quantum Information, Tsinghua University, Beijing 100084, China*

Complete contact information is available at: https://pubs.acs.org/10.1021/acs.jpclett.6c01123

Notes

The authors declare no competing financial interest.

■ ACKNOWLEDGMENTS

This work was supported by the National Natural Science Foundation of China (NSFC) (Grant Nos. 12374244 and 12341401).

■ REFERENCES

(1) Hund, F. Zur Deutung der Molekelspektren. III. Bemerkungen über das schwingungs-und rotationsspektrum bei molekeln mit mehr als zwei kernen. *Z. Phys.* **1927**, *43*, 805−826.

(2) Gurney, R. W.; Condon, E. U. Wave mechanics and radioactive disintegration. *Nature* **1928**, *122*, 439−439.

(3) Meisner, J.; Kästner, J. Atom tunneling in chemistry. *Angew. Chem., Int. Ed.* **2016**, *55*, 5400−5413.

(4) Quack, M.; Seyfang, G. Atomic and molecular tunneling processes in chemistry. In *Molecular Spectroscopy and Quantum Dynamics*; Elsevier: 2021; pp 231−282.

(5) Zhu, Y.-C.; Yang, S.; Zeng, J.-X.; Fang, W.; Jiang, L.; Zhang, D. H.; Li, X.-Z. Torsional tunneling splitting in a water trimer. *J. Am. Chem. Soc.* **2022**, *144*, 21356−21362.

(6) Kemp, J. D.; Pitzer, K. S. Hindered rotation of the methyl groups in ethane. *J. Chem. Phys.* **1936**, *4*, 749−749.

(7) Pophristic, V.; Goodman, L. Hyperconjugation not steric repulsion leads to the staggered structure of ethane. *Nature* **2001**, *411*, 565−568.

(8) Weinhold, F. A new twist on molecular shape. *Nature* **2001**, *411*, 539−541.

(9) Ryazantsev, S. V.; Feldman, V. I.; Khriachtchev, L. Conformational switching of HOCO radical: selective vibrational excitation and hydrogen-atom tunneling. *J. Am. Chem. Soc.* **2017**, *139*, 9551−9557.

(10) Pettersson, M.; Lundell, J.; Khriachtchev, L.; Räsänen, M. IR spectrum of the other rotamer of formic acid, cis-HCOOH. *J. Am. Chem. Soc.* **1997**, *119*, 11715−11716.

(11) Albert, S.; Lerch, P.; Prentner, R.; Quack, M. Tunneling and tunneling switching dynamics in phenol and its isotopomers from high-resolution FTIR spectroscopy with synchrotron radiation. *Angew. Chem., Int. Ed.* **2013**, *52*, 346−349.

(12) Schreiner, P. R.; Reisenauer, H. P.; Ley, D.; Gerbig, D.; Wu, C.-H.; Allen, W. D. Methylhydroxycarbene: Tunneling control of a chemical reaction. *Science* **2011**, *332*, 1300−1303.

(13) Lesarri, A.; Shipman, S. T.; Neill, J. L.; Brown, G. G.; Suenram, R. D.; Kang, L.; Caminati, W.; Pate, B. H. Interplay of phenol and isopropyl isomerism in propofol from broadband chirped-pulse microwave spectroscopy. *J. Am. Chem. Soc.* **2010**, *132*, 13417−13424.

(14) Ervin, K. M.; Ho, J.; Lineberger, W. C. A study of the singlet and triplet states of vinylidene by photoelectron spectroscopy of $H_2C = C^-$, $D_2C = C^-$, and $HDC = C^-$. Vinylidene−acetylene isomerization. *J. Chem. Phys.* **1989**, *91*, 5974−5992.

(15) DeVine, J. A.; Weichman, M. L.; Laws, B.; Chang, J.; Babin, M. C.; Balerdi, G.; Xie, C.; Malbon, C. L.; Lineberger, W. C.; Yarkony, D. R.; et al. Encoding of vinylidene isomerization in its anion photoelectron spectrum. *Science* **2017**, *358*, 336−339.

(16) Wenthold, P. G.; Hrovat, D. A.; Borden, W. T.; Lineberger, W. C. Transition-state spectroscopy of cyclooctatetraene. *Science* **1996**, *272*, 1456−1459.
(17) Manolopoulos, D. E.; Stark, K.; Werner, H.-J.; Arnold, D. W.; Bradforth, S. E.; Neumark, D. M. The transition state of the F+ H_2 reaction. *Science* **1993**, *262*, 1852−1855.
(18) Neumark, D. M. Transition state spectroscopy. *Science* **1996**, *272*, 1446−1447.
(19) Kim, J. B.; Weichman, M. L.; Sjolander, T. F.; Neumark, D. M.; Kłos, J.; Alexander, M. H.; Manolopoulos, D. E. Spectroscopic observation of resonances in the F+H_2 reaction. *Science* **2015**, *349*, 510−513.
(20) Weichman, M. L.; DeVine, J. A.; Babin, M. C.; Li, J.; Guo, L.; Ma, J.; Guo, H.; Neumark, D. M. Feshbach resonances in the exit channel of the F+CH_3OH→HF+CH_3O reaction observed using transition-state spectroscopy. *Nat. Chem.* **2017**, *9*, 950−955.
(21) Babin, M. C.; DeWitt, M.; Lau, J. A.; Weichman, M. L.; Kim, J. B.; Song, H.; Guo, H.; Neumark, D. M. Observation of resonances in the transition state region of the F+NH_3 reaction using anion photoelectron spectroscopy. *Nat. Chem.* **2023**, *15*, 194−199.
(22) Zhang, R.; Yan, S.; Song, H.; Guo, H.; Ning, C. Probing the activated complex of the F + NH_3 reaction via a dipole-bound state. *Nat. Commun.* **2024**, *15*, 3858.
(23) Zhang, R.; Chen, J.; Yan, S.; Jie, W.; Ning, C. Photodetachment and tunneling dissociation of cryogenic double-rydberg anions NH_4^-. *J. Phys. Chem. Lett.* **2024**, *15*, 5612−5617.
(24) Lundell, K. A.; Zhang, X.; Boldyrev, A. I.; Bowen, K. H. The existence of a designer Al = Al double bond in the $LiAl_2H_4^-$ cluster formed by electronic transmutation. *Angew. Chem., Int. Ed.* **2017**, *56*, 16593−16596.
(25) Zhang, X.; Popov, I. A.; Lundell, K. A.; Wang, H.; Mu, C.; Wang, W.; Schnöckel, H.; Boldyrev, A. I.; Bowen, K. H. Realization of an Al≡Al triple bond in the gas-phase $Na_3Al_2^-$ cluster via double electronic transmutation. *Angew. Chem., Int. Ed.* **2018**, *57*, 14060−14064.
(26) Bag, P.; Weetman, C.; Inoue, S. Experimental realisation of elusive multiple-bonded aluminium compounds: a new horizon in aluminium chemistry. *Angew. Chem., Int. Ed.* **2018**, *57*, 14394−14413.
(27) Bag, P.; Porzelt, A.; Altmann, P. J.; Inoue, S. A stable neutral compound with an aluminum−aluminum double bond. *J. Am. Chem. Soc.* **2017**, *139*, 14384−14387.
(28) Guan, S.; Shen, S.; Dou, Y.; Chen, W.; Shen, J.; Ye, B.; Cui, W.-G.; Zhong, W.; Li, Z.; Pan, H.; et al. Progress and perspectives on hydrogen storage and release in the negative hydrogen medium. *Energy Environ. Sci.* **2025**, *18*, 9324−9372.
(29) Krebsz, M.; Pasinszki, T.; Sreenath, S.; Ting, V. P. Advances in catalysing the hydrogen storage in main group metals and their tetrahydroborates and tetrahydroaluminates. *EES Catal* **2025**, *3*, 1196−1228.
(30) Tian, S. X. Ab initio study of structures and energies of Al_2H_4 and $Al_2H_4^-$. *Theor. Chem. Acc.* **2006**, *115*, 291−297.
(31) Wang, X.; Andrews, L.; Tam, S.; DeRose, M. E.; Fajardo, M. E. Infrared spectra of aluminum hydrides in solid hydrogen: Al_2H_4 and Al_2H_6. *J. Am. Chem. Soc.* **2003**, *125*, 9218−9228.
(32) Chesnut, D. B. A topological study of bonding in the Al_2H_2 and Al_2H_4 hydrides. *Chem. Phys.* **2006**, *321*, 269−276.
(33) Werner, H.; Knowles, P.; Knizia, G.; Manby, F.; Schütz, M. Wiley Interdiscip. *Rev.: Comput. Mol. Sci.* **2012**, *2*, 242−253.
(34) Larsen, N. W.; Nicolaisen, F. Far-infrared gas spectra of phenol, 4-fluorophenol, thiophenol and some deuterated species: Barrier to internal rotation. *J. Mol. Struct.* **1974**, *22*, 29−43.
(35) Tyulin, V.; Batchy-Tom, P.; Matveev, V. Improvement of the standard method for solving the problem of internal rotation in molecules with symmetrical tops. *Russ. Chem. Bull.* **1999**, *48*, 239−244.
(36) Büttiker, M.; Landauer, R. Traversal time for tunneling. *Phys. Rev. Lett.* **1982**, *49*, 1739.
(37) Steinberg, A. M. How much time does a tunneling particle spend in the barrier region? *Phys. Rev. Lett.* **1995**, *74*, 2405.
(38) Sainadh, U. S.; Xu, H.; Wang, X.; Atia-Tul-Noor, A.; Wallace, W. C.; Douguet, N.; Bray, A.; Ivanov, I.; Bartschat, K.; Kheifets, A.; et al. Attosecond angular streaking and tunnelling time in atomic hydrogen. *Nature* **2019**, *568*, 75−77.
(39) Ramos, R.; Spierings, D.; Racicot, I.; Steinberg, A. M. Measurement of the time spent by a tunnelling atom within the barrier region. *Nature* **2020**, *583*, 529−532.
(40) Vager, Z.; Naaman, R.; Kanter, E. Coulomb explosion imaging of small molecules. *Science* **1989**, *244*, 426−431.
(41) Weathersby, S.; Brown, G.; Centurion, M.; Chase, T.; Coffee, R.; Corbett, J.; Eichner, J.; Frisch, J.; Fry, A.; Gühr, M. Mega-electron-volt ultrafast electron diffraction at SLAC national accelerator laboratory. *Rev. Sci. Instrum.* **2015**, *86*, 073702.
(42) Tang, R.; Fu, X.; Ning, C. Accurate electron affinity of Ti and fine structures of its anions. *J. Chem. Phys.* **2018**, *149*, 134304.
(43) Zhang, R.; Lu, Y.; Tang, R.; Ning, C. Electron affinity of atomic scandium and yttrium and excited states of their negative ions. *J. Chem. Phys.* **2023**, *158*, 084303.
(44) Zhang, R.; Lu, Y.; Yan, S.; Ning, C. Energy levels and transition rates of the laser-cooling candidate Th^-. *Phys. Rev. A* **2025**, *111*, 023102.
(45) Kim, J. B.; Weichman, M. L.; Neumark, D. M. Low-lying states of FeO and FeO^- by slow photoelectron spectroscopy. *Mol. Phys.* **2015**, *113*, 2105−2114.
(46) Wiley, W. C.; McLaren, I. H. Time of flight mass spectrometer with improved resolution. *Rev. Sci. Instrum.* **1955**, *26*, 1150−1157.
(47) Eppink, A. T. J. B.; Parker, D. H. Velocity map imaging of ions and electrons using electrostatic lenses: application in photoelectron and photofragment ion imaging of molecular oxygen. *Rev. Sci. Instrum.* **1997**, *68*, 3477−3484.
(48) León, I.; Yang, Z.; Liu, H.-T.; Wang, L.-S. The design and construction of a high-resolution velocity-map imaging apparatus for photoelectron spectroscopy studies of size-selected clusters. *Rev. Sci. Instrum.* **2014**, *85*, 083106.
(49) Dick, B. Inverting ion images without abel inversion: maximum entropy reconstruction of velocity maps. *Phys. Chem. Chem. Phys.* **2014**, *16*, 570−580.
(50) Dick, B. MELEXIR: maximum entropy Legendre expanded image reconstruction. a fast and efficient method for the analysis of velocity map imaging or photoelectron imaging data. *Phys. Chem. Chem. Phys.* **2019**, *21*, 19499−19512.
(51) Gozem, S.; Krylov, A. I. The ezSpectra suite: An easy-to-use toolkit for spectroscopy modeling. *WIREs Comput. Mol. Sci.* **2022**, *12*, No. e1546.
(52) Wigner, E. P. On the behavior of cross sections near thresholds. *Phys. Rev.* **1948**, *73*, 1002.

https://doi.org/10.1021/acs.jpclett.6c01123
J. Phys. Chem. Lett. 2026, 17, 6405−6410